Available online at www.sciencedirect.com

ScienceDirect

journal homepage: http://www.elsevier.com/locate/acme

Original Research Article

Behavioral characteristics of hybrid girders according to type of steel–concrete connection

J.F. Choo [a], Y.C. Choi [b], W.C. Choi [c], S.W. Yoo [b,*]

[a] Department of Energy Engineering, Konkuk University, 120 Neungdong-ro, Gwangjin-gu, Seoul, 05029, Republic of Korea

[b] Department of Civil and Environmental Engineering, Gachon University, 1342 Seongnamdaero, Sujeong-gu, Seongnam-si, Gyeonggi-do, 13120, Republic of Korea

[c] Department of Architectural Engineering, Gachon University, 1342 Seongnamdaero, Sujeong-gu, Seongnam-si, Gyeonggi-do, 13120, Republic of Korea

ARTICLE INFO

Article history:
Received 10 April 2018
Accepted 25 August 2018
Available online 23 September 2018

Keywords:
Hybrid girder
Steel–concrete connection
Bending test
Strain compatibility

ABSTRACT

The design of the reinforcement in the transition zone of hybrid girders (i.e., girders composed of concrete girders and steel girders) in terms of the resistance to the transferred load is critical to ensure the integrity of the structure. Although the availability of various types of reinforcement in the transition zone, existing design guidelines are insufficient with regard to the various reinforcing methodologies. To address this shortcoming, this paper focuses on the behavioral characteristics of hybrid girders with respect to prestressing and three types of connections. Flexural tests were conducted using nine hybrid girder specimens that were designed and fabricated using different combinations of shear studs, anchors, lap joints, and prestressing techniques to achieve the steel-to-concrete connection. A numerical model also is proposed to predict the nonlinear flexural behavior of hybrid girders based on the test results and conventional strain compatibility. The results are used to evaluate the contribution of each component of the connection and derive the combination that best provides resistance for hybrid girders.

1. Introduction

The combination of steel and concrete can achieve a composite structure that is able to take full advantage of the properties of both materials. Typically, such a composite structure is composed of one or several steel girders surmounted by a reinforced concrete slab and connected by shear connection. The most common composite bridge structures are girder composite and box girder composite bridges. These configurations have been proven to be efficient for spans ranging between 30 m and 150 m in length [1]. Reinforced concrete girders are the most economical solution for short spans and steel bridges remain the best solution for longer spans due to steel's lighter

* Corresponding author.
E-mail addresses: jfchoo@konkuk.ac.kr (J.F. Choo), zerofe@gachon.ac.kr (Y.C. Choi), wchoi@gachon.ac.kr (W.C. Choi), imysw@gachon.ac.kr (S.W. Yoo).

https://doi.org/10.1016/j.acme.2018.08.008
1644-9665/

weight compared to concrete; however, steel is costlier than concrete.

In light of these features, a first attempt to combine steel girders and concrete girders was realized in 1972 with the construction of the Kurt-Schumacher Bridge in Germany, a cable-stayed bridge constructed with hybrid girders. This milestone was followed by several other outstanding examples, including the Normandy Bridge in France [2], the Tatara Bridge in Japan [3], and the Cheong-Poong Bridge in Korea [4]. The so-called hybrid girder or mixed girder in such cable-stayed bridges uses steel for the long main span and concrete for the side spans to counterweight the uplift caused by negative reactions [5–7]. A hybrid girder thus resembles a composite girder in that it combines dissimilar materials, but the difference is that the concrete and steel in a composite girder parallel each other in the longitudinal direction whereas a hybrid girder divides the concrete and steel between each end of the girder [8]. Fig. 1 presents a comparison of the structures of composite and hybrid girders.

In a hybrid girder bridge, the transition zone between the steel girder and the concrete girder must maintain continuity by sustaining large loads, including axial force, shear force, and bending and torsional moments. The transfer of such loads is generally achieved by bearing plates, shear connectors, or perfobond strip connectors [5,8]. Kim et al. [9] analyzed the efficiency of the steel-to-concrete connection of hybrid girders by considering three different connection types: (1) post-tension bars and a steel endplate, (2) post-tension bars and top, bottom, front, and back plates, and (3) flange plates and headed studs. Defining a non-dimensional efficiency factor involving the maximum moment, the volume of steel components and the yield stress of each component in the connection, Kim et al. [9] recommended the last connection type as the most efficient among the three types of detail. Note that the use of a front bearing plate was abandoned for other and more efficient alternatives after the Normandy Bridge application. He et al. [10] also studied steel–concrete connections with perfobond strips and found that, based on pushout test results, the shear capacity of one perfobond rib in a twin configuration was about 80% of a single independent perfobond rib. Oh et al. [11] considered the combined use of corrugated web and prestressing for joints and found that the accordion effect of the corrugated web improved the efficiency of prestressing the top and bottom flanges. Kozioł et al. [12] combined perfobond connectors with shear connectors and concluded that, based on the analogy to bolted and welded connections, the combination of perfobond and shear connectors improved the connection's resistance to failure.

Initially, the aim of the hybrid girder bridge design was to span obstacles in the most economical manner possible by placing steel girders and concrete girders consecutively in the longitudinal direction to reduce the bending moments in the main steel span. This aim was accomplished due to the difference in the weight of the steel (lighter) and the concrete (heavier). The hybrid girder bridge design also solved the uplift problem caused by the negative reaction force at the end supports that could occur when the side concrete span was shorter than the main span. Therefore, investigating the steel–concrete transition zone when common connections are applied seemed to be worthwhile. Accordingly, Park [5] proposed a design methodology for joints in hybrid girders that combined steel and prestressed concrete members to fill a design gap in terms of reference data and detailed design standards. Park conducted finite element analysis that considered shear stud connectors and prestressing tendons to connect a prestressed concrete girder and a steel girder. From the parametric study, it appeared that (1) the joint length was more determinant for the load–deflection relationship rather than the shear stud spacing, (2) the required minimum number of shear studs could be obtained when their spacing equaled the height of the girder section, and (3) the cracking moment of the hybrid girder was greater than that of the prestressed concrete girder when using prestressing tendons.

Because most of the aforementioned earlier studies were analytical and were intended to provide basic data for the development of design standards, the present study experimentally examines the structural behavior of hybrid girders in terms of conventional steel–concrete connections. To this end, nine hybrid girder specimens were designed and fabricated for this study using different combinations of steel–concrete connections, including shear connectors, welded anchors as perfobond connectors, lap joints, and prestressing. The used welded anchors in this study are intended to simulate a perfobond connector because of the lack of space to secure holes in the relatively small web of the steel girder. The various combinations were selected based on results obtained by Kim et al. [9], He et al. [10], Oh et al. [11], and Kozioł et al. [12]. In addition, an analytic model is proposed in this paper to predict the nonlinear flexural behavior of hybrid girders based on the experimental results and strain compatibility conditions. The analytic results agree well with the experimental data found from this study and indicate that the proposed analytic model

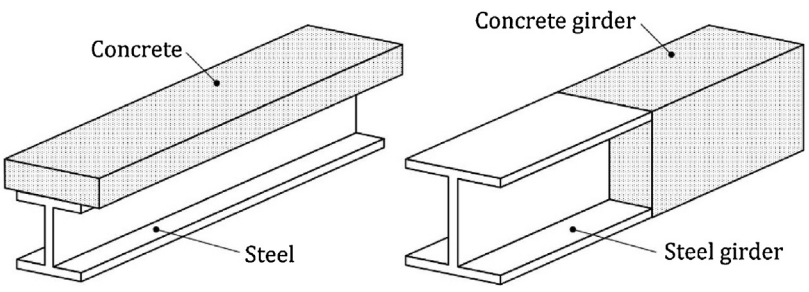

Fig. 1 – Structures of composite (left) and hybrid (right) girders.

can be used for the further development of design standards for hybrid girders using conventional steel–concrete connection methods.

2. Test setup

Fig. 2 shows the general layout and dimensions of the hybrid girder members used in this study. A total of nine members were designed and fabricated with sectional dimensions of 300 mm × 482 mm × 3400 mm and different steel–concrete connection details. In the longitudinal direction, one half of the member is made of steel and the other half is made of reinforced concrete.

2.1. *Test variables and test members*

The most suitable ways to achieve a steel–concrete connection include the use of shear connectors, perfobond connectors, and lap joints. In this study, the lap joints were realized by extending the upper and lower flanges of the H-beam of the steel girder by 250 mm in the concrete girder to form a C-shaped channel that encloses the concrete girder, as shown in Fig. 3. The perfobond connectors are simulated by anchored connections in the form of hooked bars welded to the flanges of the lap joint because of the lack of space to secure holes in the relatively small web of the steel girder. In addition, given the longitudinal composition of the girders, prestressing was chosen as the simplest method to make the steel–concrete connection.

Accordingly, the test variables are the number of shear studs, the number of welded anchors, and the level of prestressing. Table 1 lists the designations and characteristics of the nine hybrid girder members with respect to these test variables. In Table 1, f_{pu} denotes the ultimate tensile strength of the steel strand.

All the tested members utilize the same C-shaped channel lap joint of 250 mm shown in Fig. 3. The R-series members are those with prestressing and welded anchors. The S-series members achieve the steel–concrete connection via prestressing and headed shear studs. The SR-series members combine the connection types used in the R-series and S-series members. Finally, the 'Plain' member uses only a lap joint and prestressing for the steel–concrete connection.

Stepwise prestressing was applied during the fabrication of the members to minimize the elastic shortening loss. The strands were placed straight, and flexural tests were conducted immediately after prestressing so that only slip loss occurred. Taking into account both instantaneous loss and time-dependent loss, overall loss typically is around 20%–40% of the prestress force. In the present study, prestressing was applied between 70%–80% of f_{pu}. Therefore, the effective prestress force levels after loss were $0.7(1.0-0.4)f_{pu} = 0.42f_{pu}$ and $0.8(1.0-0.2)f_{pu} = 0.64f_{pu}$, which, with rounded values, give $0.4f_{pu}$ and $0.6f_{pu}$ in Table 1.

Fig. 3 includes a photograph of the studs and welded anchors used in this study. Fig. 4 presents the dimensions of the headed shear stud used in this study. Fig. 5 shows the reinforcement details of the test members listed in Table 1.

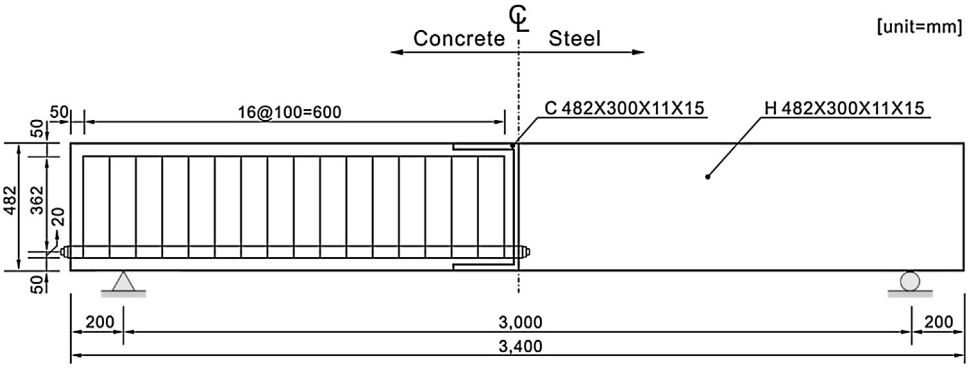

Fig. 2 – Layout and dimensions of hybrid girder members.

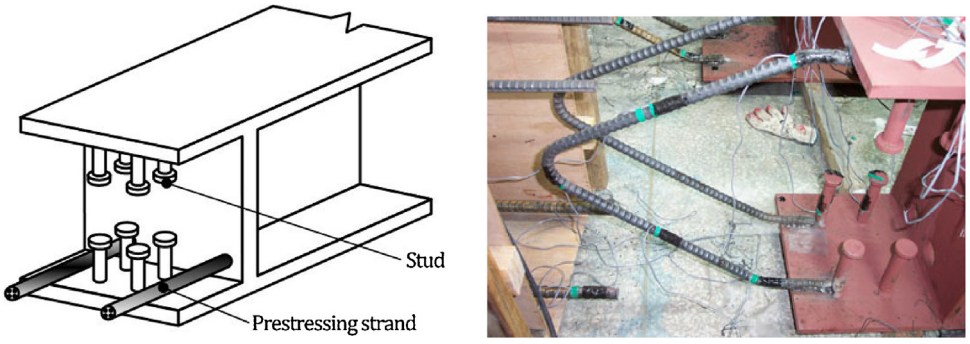

Fig. 3 – C-shaped channel lap joint with headed studs and welded anchors.

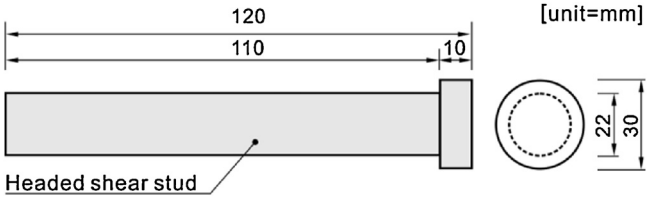

Fig. 4 – Shape and dimensions of headed shear stud.

2.2. Materials

The reinforced concrete girders were made of normal strength concrete with design strength of 40 MPa and reinforced by steel rebar with yield strength of 300 MPa. Table 2 lists the compressive strength values of the concrete measured at 7 and 28 days prior to testing. The reinforcement of the concrete girder is in accordance with the Structural Concrete Design Code of the Korea Concrete Institute [13], which limits the maximum yield strength of shear reinforcement to prevent concrete compressive crushing before the shear reinforcement yields. The material tests used the elastic modulus value of 200 GPa for the steel reinforcement and 30.37 GPa for concrete.

The steel girders used in this study were H-beams (H-482 × 300 × 11 × 15 mm) made of SS400 steel with yield strength of 260 MPa. The studs also were made of SS400. Prestressing was performed using SWPC-7-B strands with diameter of 15.2 mm, yield strength f_{py} of about 1600 MPa, tensile strength f_{pu} of about 1900 MPa, that were placed in two sets of four bundles at the bottom left and right sides of the concrete section to total eight strands (Figs. 5 and 6). The material test guidelines recommend an elastic modulus value of 200 GPa for the steel girder and the prestressing strands.

2.3. Sensor layout

For the measurements taken during the three-point bending tests of all the girders listed in Table 1, sensors were placed at various locations on the test members. Strain gauges were installed on the tensile reinforcement, welded anchors, studs, and concrete. The load cell of the actuator was used to record the load. One linear variable differential transducer (LVDT) was installed to measure the deflection at the center, and two other LVDTs were placed on the left and right sides of the center to measure the deflections of the concrete girder and steel girder, respectively. Fig. 7 presents the layout of the sensors with their locations.

3. Test results and discussion

All the test members were subjected to static three-point bending tests to failure using an actuator of 2000 kN. With the supported span length of 3000 mm, the load was applied to the center of the member (Fig. 8).

The results presented in Table 3 reveal that the rupture load of the studs was slightly higher than that of the welded anchors. The rupture load in the SR-series members that concurrently used studs and anchors for the steel–concrete connection led to clearly larger values than for the S-series and R-series members and was similar to the failure load of the member. Here also, the welded anchors broke before the studs. With regard to the failure load, the Plain member without studs and anchors failed at lower load levels than the other test members. The S-series members developed slightly higher resistance to failure than the R-series members. However, the failure load seems to have been more dependent on the prestressing level than the applied load. The concurrent use of studs and anchors increased the crack load, the rupture load of the studs and anchors, and the failure load. The failure of the SR-series members started from the rupture of the studs. Member SR2 failed at a slightly lower load level than member SR1 due to fewer studs in the connection for the SR2 member.

3.1. Crack and failure patterns of hybrid girder members

Based on the results presented in Table 3, the cracking load of the hybrid girder members ranged between 142.3 kN and 284.7 kN. The largest value, which was observed for the Plain member, indicates that prestressing alone did not achieve the composite behavior of the steel and concrete girders until very substantial loading was applied. In addition, the concurrent use of both shear connectors and welded anchors appears to have delayed cracking compared to the separate use of studs or anchors.

Fig. 9 presents the crack patterns of the hybrid girder members. All the cracks initiated in the concrete at the bottom of the steel–concrete connection and propagated upward with increasingly heavier loads before exhibiting typical flexural crack patterns. Shear cracks occurred prior to failure in the concrete inside the connection. Most of the crack widths remained smaller than 0.5 mm, but the number of cracks at failure differed according to the type of steel–concrete connection. The Plain member experienced very few cracks, followed by the R-series members, and the S-series members showed numerous cracks at failure. The large number of cracks in the S-series members can be attributed to the studs, which maintained the steel–concrete connection until failure. On the other hand, the welded anchors sustained the connection only until they ruptured. Moreover, the crack patterns of the S-series and SR-series members indicate that near-to-perfect composition can be achieved when numerous studs are used and the prestress level is great.

Fig. 10 presents the failure patterns of the members by type of connection. The progression of failure in all the members started with the rupture of the welded anchors, followed by that of the studs, and finally by the plastic deformation of the C-channel lap joint. The studs ruptured due to the flexural deformation of the shaft, followed by the rupture of the weld. Fig. 11 shows details of the failure of each component of the steel–concrete connections.

3.2. Load–deflection curves

3.2.1. Effect of welded anchors

Given that the welded anchors are intended to simulate perfobond connectors, Fig. 12 presents a comparison of the load–deflection curves of the R-series members: R1, R2, and R3. These three members have the same level of prestress ($0.6f_{pu}$) but different arrangements of the welded anchors. The load–deflection of Plain member P1 with only prestressing ($0.6f_{pu}$) is also plotted to show the effect of the welded anchors on the

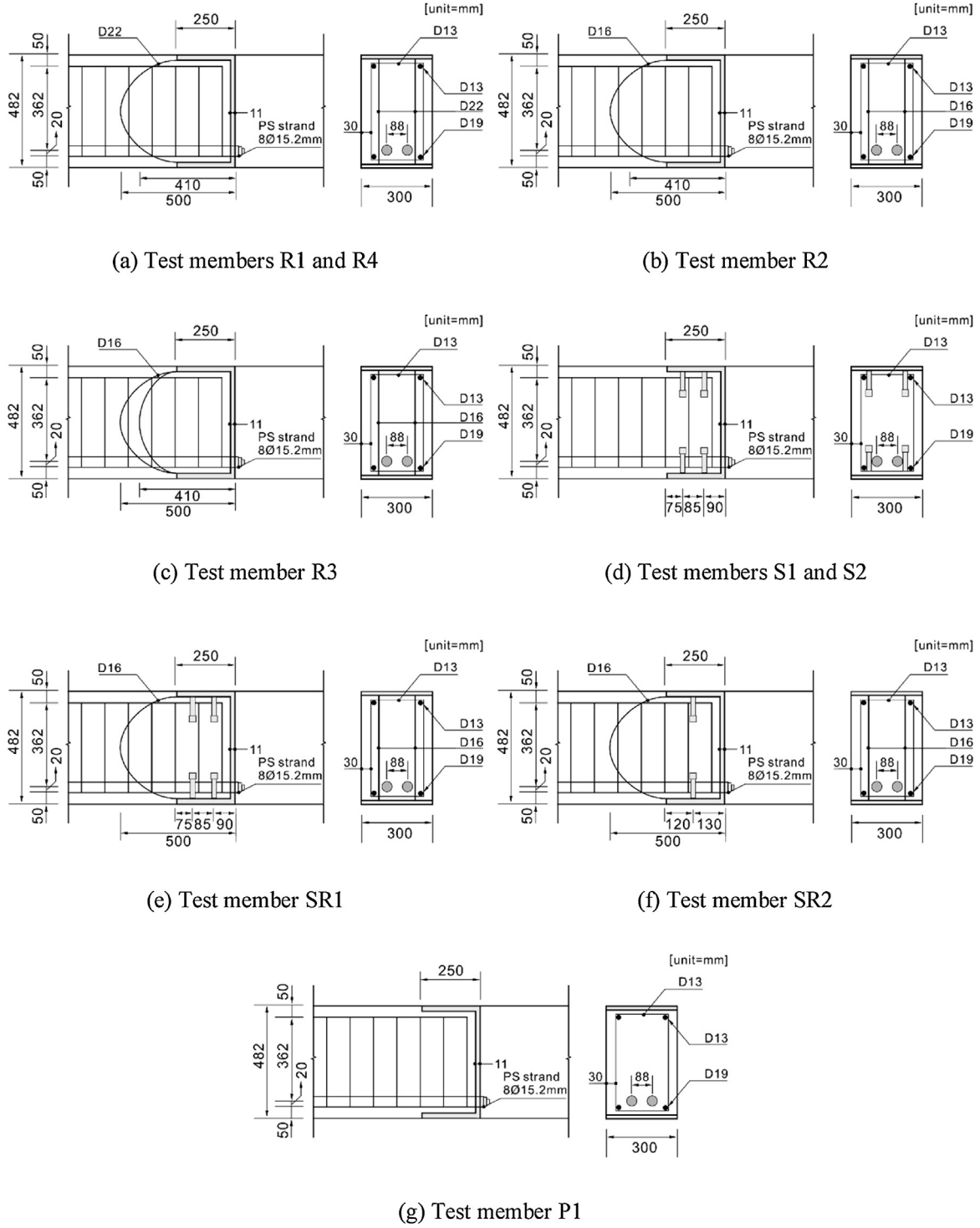

Fig. 5 – Reinforcement details of hybrid girder test members.

behavior of the hybrid girder. All the R-series members did not develop noticeable resistance after the rupture of the anchor welds. First, the load–deflection curve of member R2 with two D16 anchors is practically identical to that of member P1, which indicates that the welded anchors of member R2 did not provide particular improvement of the performance of the transition zone between the concrete girder and the steel girder. In addition, members R1 and R3 with two D22 anchors and three D16 anchors, respectively, exhibited improved performance of the steel–concrete connection with similar behavior. This similarity can be explained by the fact that near-to-perfect composition is ensured when the total area of the bars exceeds 595.8 mm^2 (R3); for members R1 and R2, these areas are 774.2 mm^2 and 595.8 mm^2, respectively. Compared

Table 1 – Designation and characteristics of hybrid girder test members.

Designation	Anchor rebar/stud (number)	Prestress force
R1	Anchor D22 (2)	$0.6f_{pu}$
R2	Anchor D16 (2)	$0.6f_{pu}$
R3	Anchor D16 (3)	$0.6f_{pu}$
R4	Anchor D22 (2)	$0.4f_{pu}$
S1	Stud ϕ22 (8)	$0.6f_{pu}$
S2	Stud ϕ22 (8)	$0.4f_{pu}$
SR1	Anchor D16 (2) + Stud ϕ22 (8)	$0.6f_{pu}$
SR2	Anchor D16 (2) + Stud ϕ22 (4)	$0.6f_{pu}$
P1 (Plain)	–	$0.6f_{pu}$

Table 2 – Material test results of concrete.

Design strength (MPa)	Compressive strength (MPa)			Slump (cm)	Entrained air (%)
	7 days	28 days	Before test		
40.0	34.8	40.6	45.6	13	2.6

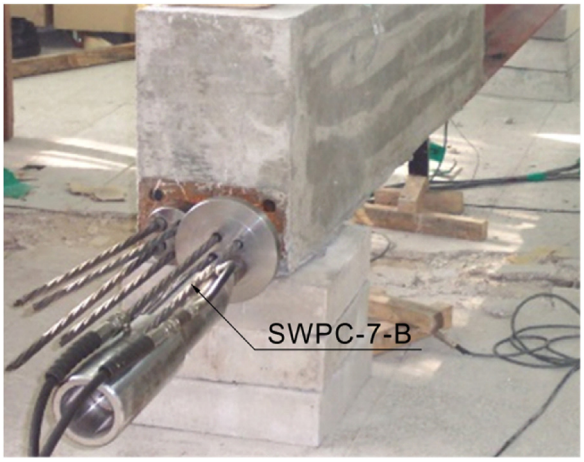

Fig. 6 – Prestressing of steel–concrete connection in hybrid girder test member.

to member P1, members R1 and R3 improved the flexural resistance of the hybrid girder by about 91%–130%, respectively, before their rupture.

In view of the experimental data, rather than the area of the welded anchors, their length in the steel–concrete connection seems to be most determinant in the behavior of the hybrid girder. In terms of perfobond connectors, this finding implies the existence of a limited size of the perfobond rib connector, which would help determine whether the dowel effect can or cannot be expected to contribute to the behavior of the steel-to-concrete connection.

3.2.2. *Effect of studs*

As mentioned in Section 3.1, the studs developed greater resistance to rupture than the welded anchors. Comparing members S2 and S1 with the same number of studs but different levels of prestress in Fig. 13, the increase in prestress from $0.4f_{pu}$ to $0.6f_{pu}$ is shown to improve the effect of the studs on the load resistance of the steel–concrete connection.

The SR-series members with two D16 welded anchors and the same level of prestress ($0.6f_{pu}$) have different numbers of studs: eight studs for SR1 and four studs for SR2. As discussed in Section 3.1, the concurrent use of both welded anchors and shear studs significantly increased the crack load, rupture load, and failure load compared to the S-series and R-series members. Moreover, the failure of the SR-series members started from the rupture of the studs. In short, the use of more studs increased the load resistance of the hybrid girder member.

3.2.3. *Effect of prestress*

In Figs. 12–14 for the load deflection of the Plain member using only prestressing and the C-channel lap joint for the steel–concrete connection, the largest deflection occurred at the center of the beam, with slightly larger values for the concrete portion than for the steel. This occurrence can be explained by the short length of the C-channel lap joint. Furthermore, the Plain member without studs and anchors failed at lower load levels than the other members, which indicates that prestressing alone cannot achieve the composition of the steel and concrete girders unless very substantial loading is applied.

The comparison of members R1 and R4, which have the same number and type of welded anchors but different levels of prestress ($0.6f_{pu}$ and $0.4f_{pu}$), shows that the higher level of prestress improves the role of the welded anchors in terms of the resistance of the steel–concrete connection. The comparison of members S1 and S2, which have the same number of ϕ22 studs, reveals that the increase in prestress force from $0.4f_{pu}$ to $0.6f_{pu}$ allows the member to continue to resist failure even after the studs have ruptured. The same observation can be made when comparing members SR1 and SR2. Consequently, increasing the level of prestress seems appropriate for developing a greater effect of the studs.

3.3. *Load–strain curves*

3.3.1. *Load–strain relationship in reinforced concrete girders*

Fig. 15 presents the load–strain curves measured by the rebar strain gauges located at the end of the tensile reinforcement of the concrete girder for the steel–concrete connection shown in Fig. 7(a). All the members experienced yielding of their tensile reinforcement at the mid-span of the hybrid girder. Of particular note is that the strain levels of the tensile reinforcement ranged between 1800 and 5300 με at the ultimate state of the members; these strain levels are significantly lower than typically observed for common flexural members. This finding indicates that, after the yielding of the tensile reinforcement, the members experienced failure due to the rupture of either the studs or the welded anchors. The welded anchors did not yield because the welds broke before the anchors could be effective. Compared to member P1, the welded anchors in the R-series members slightly delayed the yielding of the tensile reinforcement, but their premature rupture did not help the tensile reinforcement to contribute to the flexural resistance of the hybrid girder. The curves for members R1 and R4 show that a higher level of

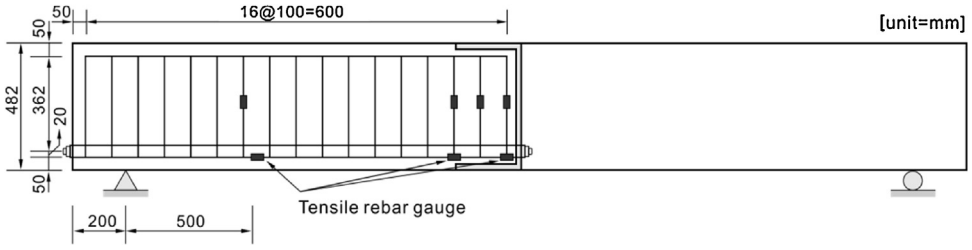

(a) Layout of sensors installed inside the test member

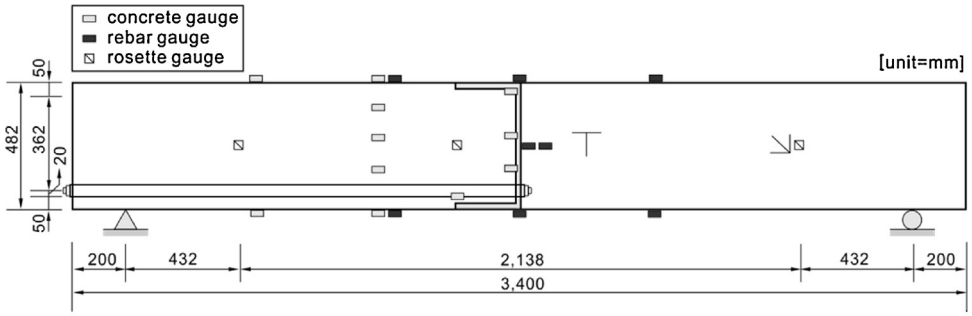

(b) Layout of sensors installed outside the member

Fig. 7 – Layout of sensors installed on test members.

Fig. 8 – Three-point bending test of hybrid girder test member.

prestress is necessary for the welded anchors to play a role in the steel–concrete connection. In comparison, the studs in the S-series and SR-series members are seen to promote the composition between the steel and concrete girders and help the tensile reinforcement fulfill its role in the flexural resistance of the hybrid girder. The load–strain curves of the concrete that are plotted concurrently in Fig. 15 correspond to those measured by the strain gauge located at the upper corner of the concrete girder in the steel–concrete connection shown in Fig. 7(b). It appears that the strain at the top fiber of the concrete increased significantly after 0.0035 for the member with a low prestress level (R4) and those without and with a small area of welded anchors (P1 and R3, respectively). Thus, the upper steel fiber fully sustained the compressive force after the concrete reached its ultimate strain of 0.0035.

3.3.2. *Load–strain relationship in steel girders*

Fig. 16 presents the load–strain curves measured at the top (left) and bottom (right) of the steel girder part of the hybrid girder. The plotted values are the ones measured at the steel–concrete connection of the hybrid girders. The steel girder surrounding the steel–concrete connection of the hybrid girder exhibited the stress state of a typical flexural member at early loading. However, after the plastic deformation of the C-channel lap joint, the behavior appears to deviate from that of a typical flexural member. Moreover, the steel around the steel–concrete connection yielded nonlinearly, which indicates that the steel bore a large portion of the load.

4. Analytic model and comparison with experimental data

This Section 4 proposes an analysis model to simulate the nonlinear flexural behavior of a hybrid girder. The model assumes strain compatibility and full composition via prestressing. The results simulated by the analytic model are then compared to this study's experimental data for validation.

4.1. *Proposed analysis model for nonlinear flexural behavior of hybrid girder*

The concrete model adopted here is the nonlinear model proposed by Hognestad [14] and expressed as Eq. (1). A bilinear model is used for the reinforcement and steel girder to

Table 3 – Crack load, stud/welding rupture load and failure load of hybrid girder members under static loading test.

Test member	Measured loads (kN)				Failure pattern
	Crack	Rupture of welded anchors	Rupture of shear studs	Failure	
R1	160.1	461.7	–	659.2	Failure of lap joint by plastic deformation after rupture of welded anchors
R2	177.9	338.1	–	526.7	
R3	142.3	382.6	–	644.1	
R4	195.7	302.5	–	532.9	
S1	213.5	–	466.2	719.7	Failure of lap joint by plastic deformation after rupture of shear studs
S2	195.7	–	490.2	572.0	
SR1	266.9	649.4	670.8	715.3	Failure of lap joint by plastic deformation after rupture of welded anchors and shear studs
SR2	266.9	626.3	631.7	631.7	
P1	284.7	–	–	538.2	Failure of lap joint by plastic deformation

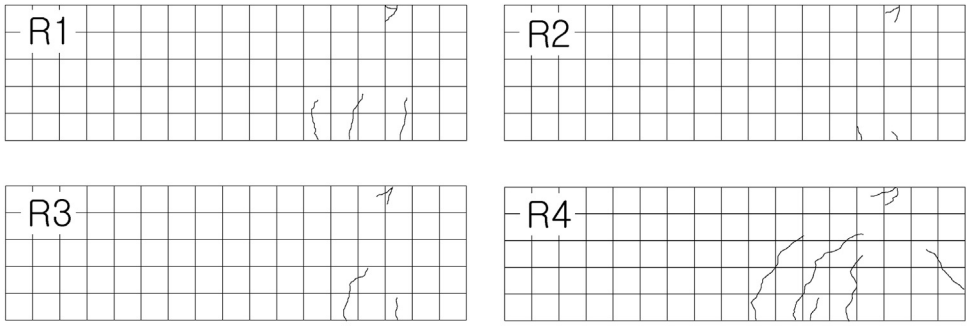

(a) R-series members

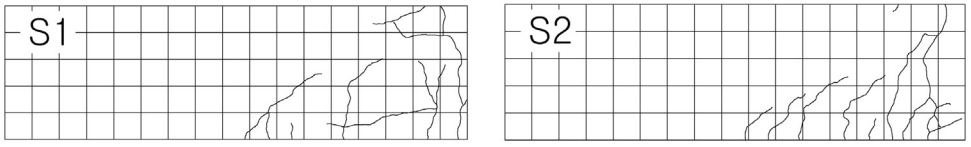

(b) S-series members

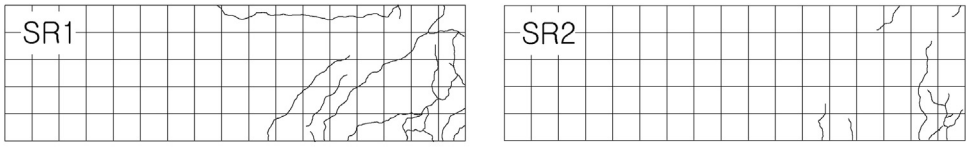

(c) SR-series members

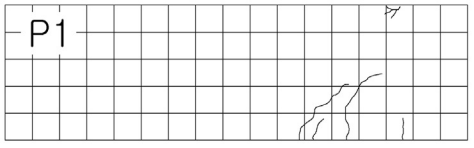

(d) Plain member

Fig. 9 – Crack patterns in concrete girder of hybrid girder test members.

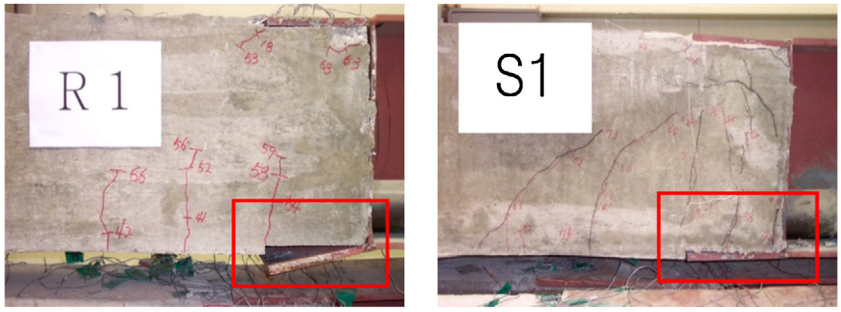

(a) Member R1 (b) Member S1

(c) Member SR2 (d) Plain member

Fig. 10 – Failure patterns of hybrid girder test members.

(a) Deformation of stud (b) Rupture of stud weld

(c) Rupture of anchor weld (d) Deformation of C-channel lap joint

Fig. 11 – Details of failure in steel–concrete connections of hybrid girder test members.

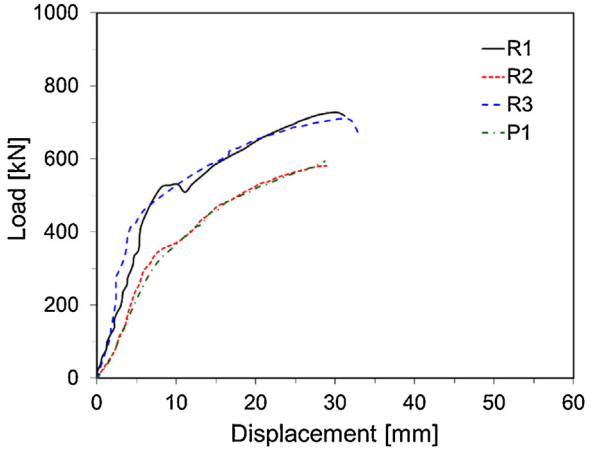

Fig. 12 – Load–deflection curves measured for R-series members.

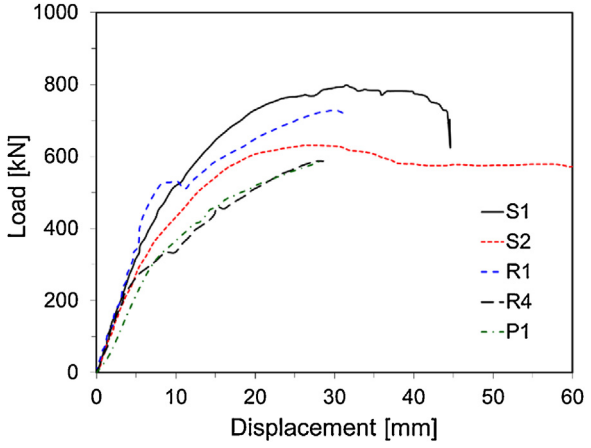

Fig. 13 – Load–deflection curves measured for S-series members.

consider the post-yielding elastic modulus values of the reinforcement and steel girder.

$$f_c = f_c''\left[\frac{2\epsilon}{\epsilon_0} - \left(\frac{\epsilon}{\epsilon_0}\right)^2\right] \quad \text{where } \epsilon_0 = \frac{2f_c''}{E_c} \tag{1}$$

where f_c = concrete stress; ϵ = concrete strain corresponding to f_c; f_c'' = peak concrete stress (MPa); ϵ_0 = ultimate strain or strain corresponding to f_c''; and E_c = initial elastic modulus of concrete (MPa).

With regard to the strain compatibility conditions, the strain in the compressive zone of the section, ϵ_c, is increased stepwise from early loading to failure. At each step, the corresponding stress levels in the steel and concrete, the flexural strength, and the curvature are computed. The concept is illustrated in Fig. 17 and formulated in Eqs. (2) and (3).

For the reinforced concrete cross-section with height h and width b shown in Fig. 17, ϵ_{s1} is the strain in the top steel fiber, ϵ_s' is the strain in the compressive reinforcement, ϵ_p is the strain

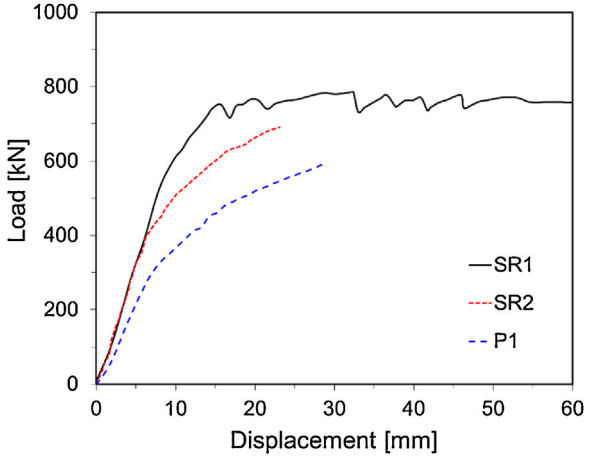

Fig. 14 – Load–deflection curves measured for SR-series members.

in the prestressing tendon, ϵ_s is the strain in the tensile reinforcement, and ϵ_{s2} is the strain in the bottom steel fiber. These strains can be expressed as follows:

$$\begin{aligned}
\epsilon_{s1} &= \frac{c + \frac{1}{2}t_t}{c}\epsilon_c \\
\epsilon_s' &= \frac{c - d' + t_t}{c}\epsilon_c \\
\epsilon_p &= \frac{d_p - c - t_t}{c}\epsilon_c \\
\epsilon_s &= \frac{d - c - t_t}{c}\epsilon_c \\
\epsilon_{s2} &= \frac{h - c - t_t - \frac{1}{2}t_b}{c}\epsilon_c
\end{aligned} \tag{2}$$

where d = depth of the tensile steel from the top of the section; d_p = depth of the prestressing tendon from the top of the section; d' = depth of the compressive steel from the top of the section; c = depth of the neutral axis from the top of the section; t_t = thickness of the top flange; and, t_b = thickness of the bottom flange.

For a given strain, the stress level in the concrete is obtained using the concrete model of Hognestad shown in Eq. (1), and the stress level in the tensile steel can be obtained using the bilinear behavioral model. Therefore, the resultant forces that correspond to the strains in Eq. (2) and shown in the stress distributions shown in Fig. 17 can be obtained as expressed in Eq. (3).

$$\begin{aligned}
C_{s1} &= \int_{A_{s1}} f_{s1}\,dA_{s1} = A_{s1}f_{s1} \\
C_s' &= \int_{A_s'} f_s'\,dA_s' = A_s'f_s' \\
C_c &= \int_{A_c} f_c\,dA_c = A_c f_c \\
T_p &= \int_{A_p} f_p\,dA_p = A_p f_p \\
T_s &= \int_{A_s} f_s\,dA_s = A_s f_s \\
T_{s2} &= \int_{A_{s2}} f_{s2}\,dA_{s2} = A_{s2}f_{s2}
\end{aligned} \tag{3}$$

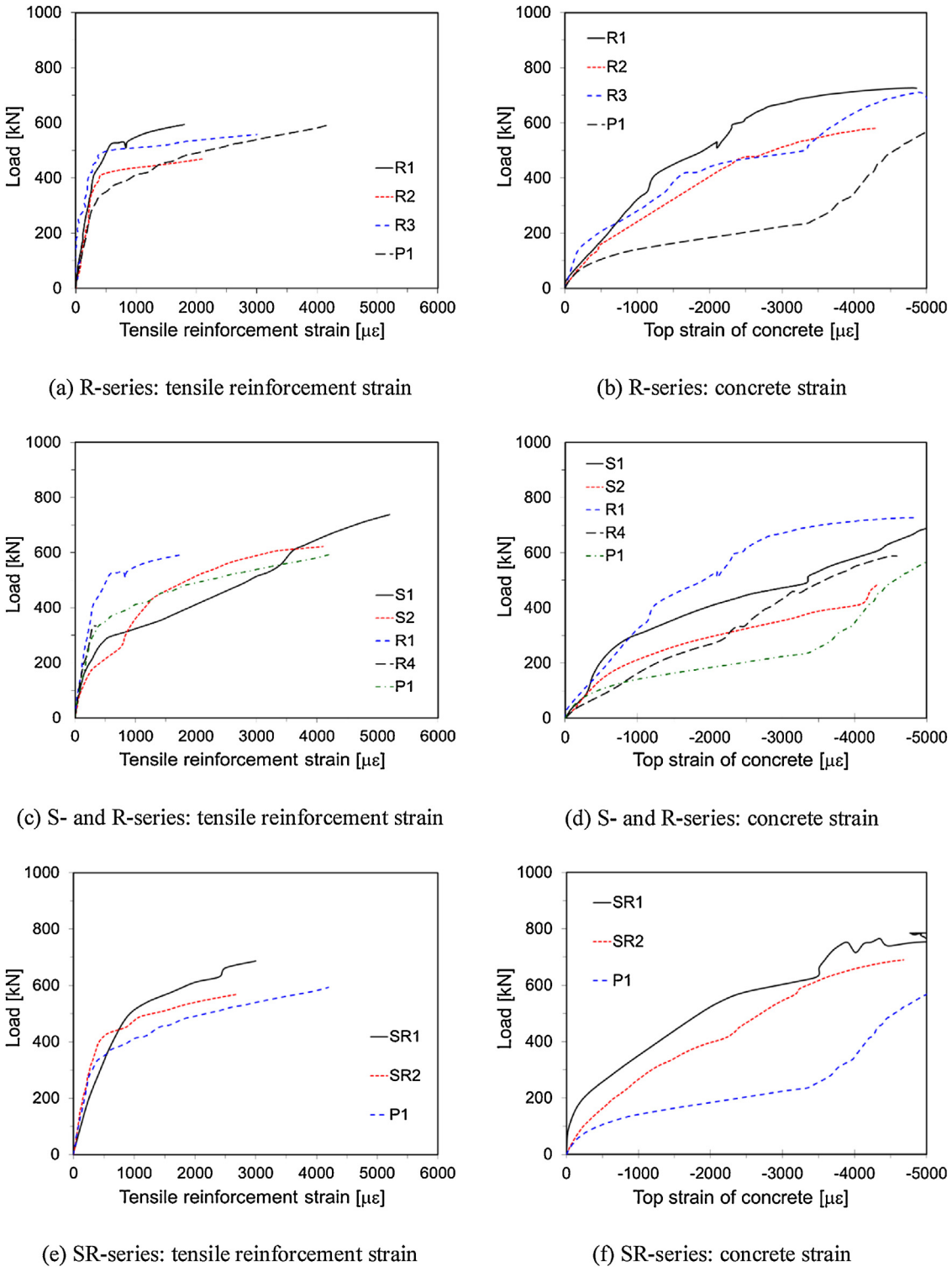

(a) R-series: tensile reinforcement strain

(b) R-series: concrete strain

(c) S- and R-series: tensile reinforcement strain

(d) S- and R-series: concrete strain

(e) SR-series: tensile reinforcement strain

(f) SR-series: concrete strain

Fig. 15 – Load–strain curves measured for concrete girders.

where A_{s1} and f_{s1} = area and stress of the top flange, respectively; A_{s2} and f_{s2} = area and stress of the bottom flange, respectively; A'_s and f'_s = area and stress of the compressive reinforcement, respectively; A_c = area up to ϵ_c under the Hognestad model stress–strain curve for concrete; A_p and f_p = area and stress of the prestressing tendon, respectively; and, A_s and f_s = area and stress of the tensile reinforcement, respectively.

Expressing the equilibrium of these resultant expressions gives Eq. (4).

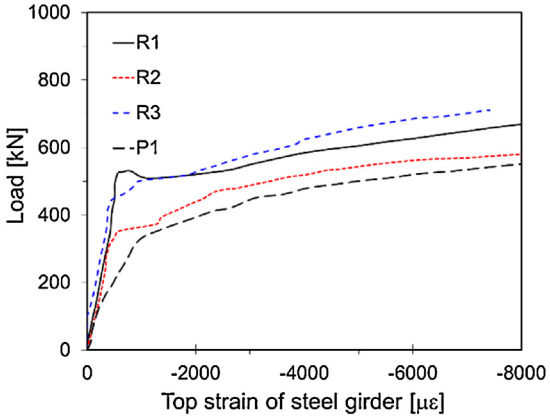

(a) R-series: top of steel girder

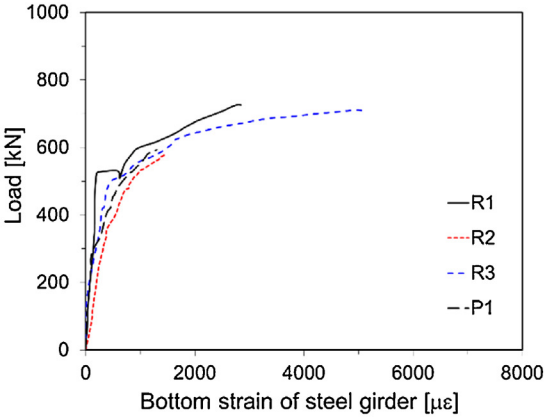

(b) R-series: bottom of steel girder

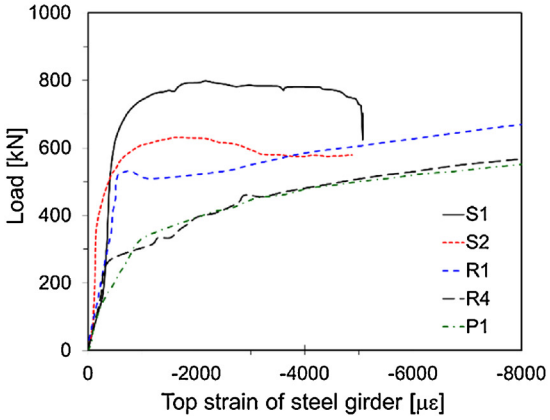

(c) S- and R-series: top of steel girder

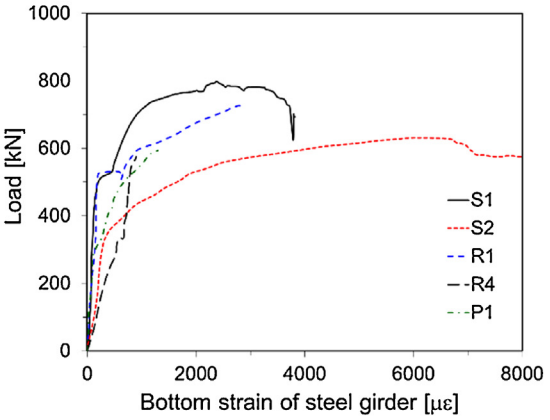

(d) S- and R-series: bottom of steel girder

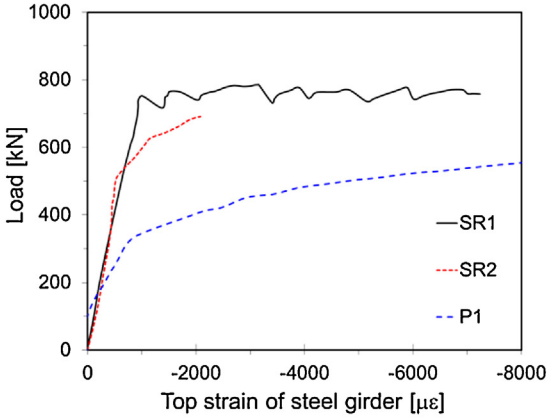

(e) SR-series: top of steel girder

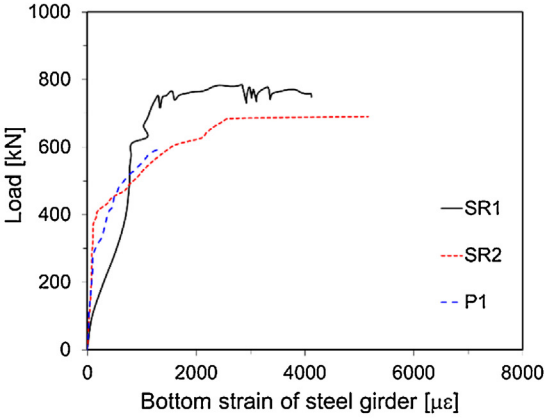

(f) SR-series: bottom of steel girder

Fig. 16 – Load–strain curves measured for steel girders.

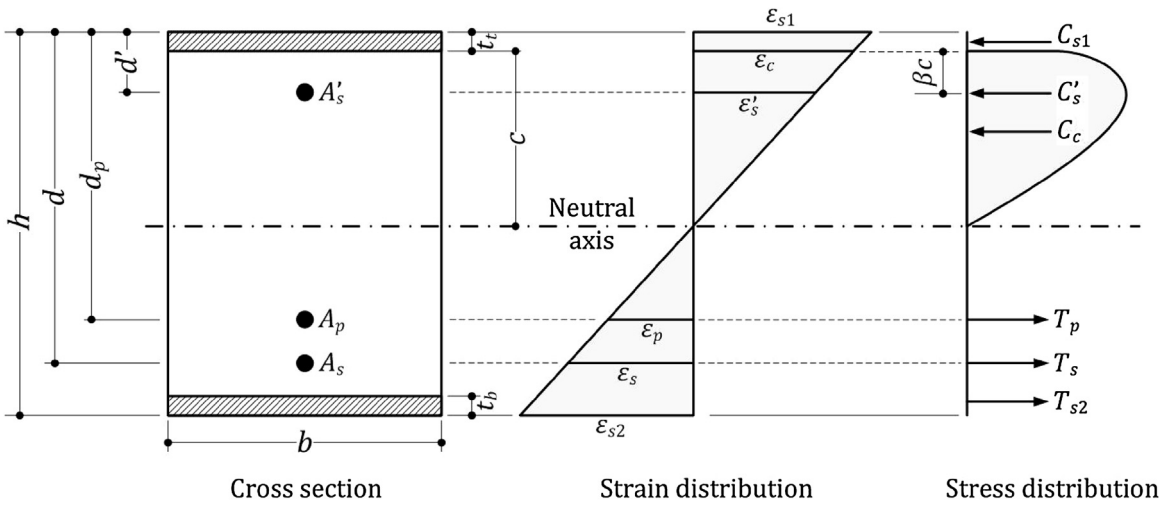

Fig. 17 – Strain compatibility of cross-section for analysis.

$$N = C_{s1} + C'_s + C_c + T_p + T_s + T_{s2} = 0. \quad (4)$$

The resisting moment of the cross-section can be obtained by means of the moments of the forces expressed in Eq. (3) by Eq. (5).

$$M = \left(c + \frac{1}{2}t_t\right)C_{s1} + (c + t_t - d')\,C'_s + \left(c - \frac{1}{2}\beta\right)C_c + (d_p - c - t_t)T_p + (d - c - t_t)T_s + \left(h - c - t_t - \frac{1}{2}t_b\right)T_{s2} \quad (5)$$

where β = centroid factor of the concrete stress distribution.

Finally, the curvature ϕ, deflection Δ, and load P can be obtained using the span length L and the flexural strength, as shown in Eqs. (6)–(8), respectively.

$$\phi = \frac{\epsilon_c}{c} \quad (6)$$

$$\Delta = \sin^{-1}\left(\frac{L\phi}{2}\right) \quad (7)$$

$$P = \frac{4M}{L} \quad (8)$$

4.2. *Validation of analytic model and discussion*

4.2.1. *Load–deflection curves*

Fig. 18 compares the load–deflection curves obtained experimentally to those predicted by the analytic model assuming perfect bonding. Members R1, R3, S1, SR1, and SR2 developed greater resistance than those predicted by the analysis. This outcome indicates that these members are characterized by a prestress level that is higher than $0.6f_{pu}$ and an area of the welded anchors that is larger than 595.8 mm^2 (R3, 3-D16) and that eight studs or four studs with an area of the welded anchors that is larger than 397.2 mm^2 (2-D16) could secure perfect bonding behavior. These observations were used to assess the resistance to flexure of the hybrid girder with respect to horizontal shear force, the cross-sectional area of the studs or welded anchors, and the prestress force.

4.2.2. *Evaluation of shear connectors*

The horizontal shear force V_{hor} that acts on concrete is calculated using the ultimate load obtained from testing. The so-calculated horizontal shear force is then compared to the resistance of the shear stud to assess the eventual failure of the stud using Eqs. (9) and (10).

$$V_{hor} \le V_{stud} + V_{anchor} + V_{ps} \quad (9)$$

$$V_{anchor} = U\sqrt{f'_c}\,A_{anchor} \quad (10)$$

where V_{stud}, V_{anchor}, and V_{ps} = shear force of the studs, welded anchors, and prestressing, respectively; A_{anchor} = apparent area of the welded anchor bar; and U = bond strength of the welded anchor (MPa).

The formula proposed by Orangun et al. [15] is adopted here to account for the effect of the bond strength that stems from the use of the welded anchors. Orangun et al. [15] pointed out that the use of American Concrete Institute (ACI) 408R [16] underestimates the concrete bond strength; so, they conducted pullout tests to derive Eq. (11) that considers the effects of the compressive strength of concrete, the cover thickness, the diameter of the rebar, and the developed length on the bond strength.

$$\frac{U}{\sqrt{f'_c}} = 0.1 + 0.25\frac{C_{min}}{d_b} + 4.15\frac{d_b}{l_d} \quad (11)$$

where $U/\sqrt{f'_c}$ = bond strength factor; f'_c = measured compressive strength of concrete (MPa); C_{min} = minimum cover thickness (mm); d_b = rebar diameter (mm); and l_d = developed length (mm).

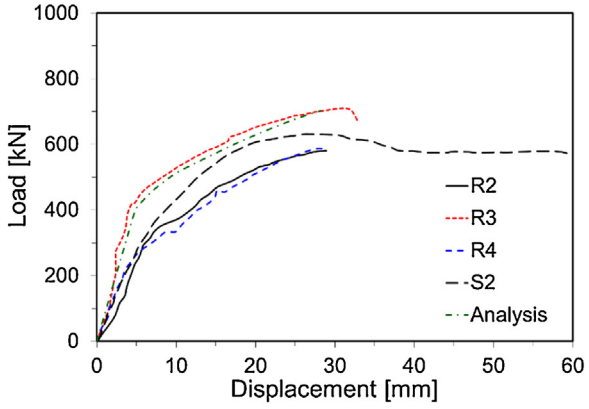

(a) R-series data

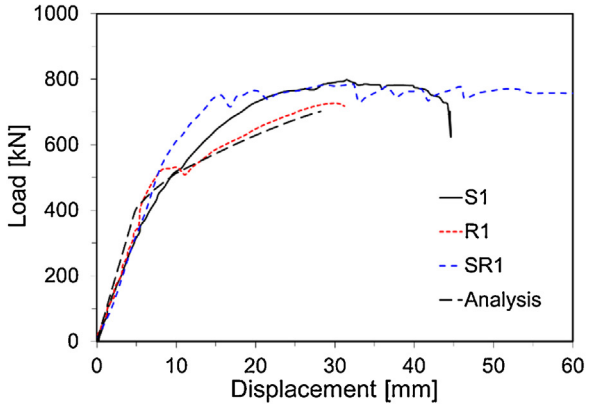

(b) Members with near-to-perfect bonding

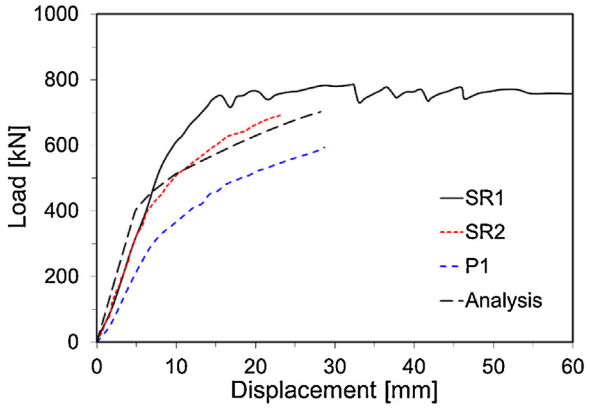

(c) SR-series data

Fig. 18 – Comparison of experimental and analytic load–deflection curves.

The resistance of the headed shear stud suggested by Eurocode [17,18] and the American Association of State Highway and Transportation Officials (AASHTO) [19] is as follows. Eurocode-4 [17,18] recommends that the smallest value between Eqs. (12) and (13) should be the design shear resistance of the headed shear connector.

$$V_{stud} = P_{RD} = \frac{0.8 f_u \frac{\pi d^2}{4}}{\gamma} \tag{12}$$

$$V_{stud} = P_{RD} = \frac{0.29 \alpha d^2 \sqrt{f_{ck} E_{cm}}}{\gamma} \tag{13}$$

where γ = partial factor (1.25); d = stud shank diameter; f_u = specified ultimate tensile strength of the material of the stud; f_{ck} = compressive strength of concrete; E_{cm} = elastic modulus of concrete; and

$$\alpha = \begin{cases} 0.2\left(\frac{h_{sc}}{d}+1\right) & \text{for } 3 \le h_{sc} \le 4 \\ 1 & \text{for } \frac{h_{sc}}{d} > 4 \end{cases} \tag{14}$$

where h_{sc} = overall nominal height of the stud.

In addition, AASHTO LRFD (Load and Resistance Factor Design) [19] recommends Eq. (15) for the nominal shear resistance of one stud shear connector embedded in a concrete deck.

$$V_{stud} = Q_r = \phi_{sc} Q_n = \phi_{sc} 0.5 A_{sc} \sqrt{f_c' E_c} \le \phi_{sc} F_u A_{sc} \tag{15}$$

where ϕ_{sc} = resistance factor; A_{sc} = cross-sectional area of the stud; E_c = elastic modulus of concrete; and F_u = minimum specified tensile strength of one stud. Note that, for clarity, this study adopted the values recommended by Eurocode and did not consider the safety factor.

Finally, the shear force provided by the prestressing strand is calculated as expressed in Eq. (16).

$$V_{ps} = f_{pe} A_p \tag{16}$$

where f_{pe} = effective prestress force and A_p = area of the prestressing strand.

Table 4 compares the contribution of each steel–concrete connection component using Eqs. (9)–(16) to assess the role of each of these components in the resistance of the hybrid girder. The last column in the table indicates whether the computed resistance fails or does not satisfy Eq. (9).

According to the presented results, the shear connection failed in all the members with the exception of the SR-series. However, the members with greater resistance provided by the design codes exhibited better structural performance than the numerically predicted members assuming perfect bonding. Even if the SR-series members were predicted to develop sufficient resistance without failure of the shear connection, premature failure nonetheless occurred because the welds of the anchors ruptured. That is, the member would not have failed due to the rupture of the shear connection in the case of real perfobond connectors. Even if the bond strength values provided by previous test results were applied to compute the resistance of the welded anchors that were assumed as perfobond connectors in Table 4, further studies should more closely examine the resistance of welded anchors.

Table 4 – Contribution of studs, welded anchors and prestressing strand (PS) in the performance of the steel–concrete connection of the hybrid girder.

Member	Ult. load	Moment	Avg. concrete stress	Horiz. shear force	Shear resistance				$V_{hor} < V_r$
					Stud	Anchor	PS	Total	
	P_u	M	f_a	V_{hor}	V_{stud}	V_{anchor}	V_{ps}	V_r	
	kN	kN m	MPa	kN	kN	kN	kN	kN	
R1	659.2	494.400	39.91	5411.8	–	2329.1	1264.9	3594.0	N.G
R2	526.7	395.025	31.89	4324.3	–	2262.7	1264.9	3527.6	N.G
R3	644.1	483.075	39.00	5288.4	–	3394.1	1264.9	4659.0	N.G
R4	532.9	399.675	32.27	4375.8	–	2329.1	843.3	3172.4	N.G
S1	719.7	539.775	43.58	5909.4	3411.5	–	1264.9	4676.4	N.G
S2	572.0	429.000	34.63	4695.8	1705.7	–	843.3	2549.0	N.G
SR1	715.3	536.475	43.31	5872.8	3411.5	2262.7	1264.9	6939.1	O.K
SR2	631.7	473.775	38.25	5186.7	3411.5	2262.7	1264.9	6939.1	O.K
P1	538.2	403.650	32.59	4419.2	–	–	1264.9	1264.9	N.G

5. Conclusions

Defining a hybrid girder as a structure that combines dissimilar materials in the longitudinal direction, the present study experimentally examined the structural behavior of hybrid girders that combined a concrete girder and a steel girder and considered conventional steel–concrete connections in order to provide basic data for the development of design standards. To that end, bending tests were conducted in this study using nine hybrid girder specimens that were designed and fabricated using different combinations of steel–concrete connections: shear stud connectors, welded anchors as perfobond connectors, lap joints, and prestressing. In addition, after completing section analysis with strain compatibility, an equation which is able to compare with analysis results for perfect bonding case was proposed to determine the resistance of composite structure by using the existing design equation of the shear connector, the equation for bond strength of the welded anchor, and the equation of shear resistance for prestressing. The following conclusions can be drawn from the results.

(1) The number of cracks at failure differed according to the type of steel–concrete connection. The crack patterns of the members with shear studs or a combination of shear studs and welded anchors led to near-to-perfect composite action of the members when the number of studs and the prestress level were both high. The concurrent use of both shear connectors and welded anchors appeared to delay the occurrence of cracking compared to the exclusive use of studs or anchors.
(2) The concurrent use of studs and welded anchors also increased the rupture load of the studs and welded anchors and the failure load of the hybrid girder. The progress of failure in all the members started with the rupture of the welded anchors, followed by that of the studs, and finally by the plastic deformation of the lap joint.
(3) In view of the experimental data, rather than the area of the anchors, the length of the welded anchor and the weld length in the steel–concrete connection seemed to be the most determinant factors of the effect of the welded anchor on the behavior of the hybrid girder.
(4) After completing section analysis with strain compatibility under perfectly bonded cases, a comparison of the analytic results with the experimental data showed that the members with a steel–concrete connection combined with a high prestress level, a large area of the welded anchors mixed with any studs could secure perfect bonding behavior.
(5) The contribution of each component in the steel–concrete connections was calculated, and the results showed that the members with the most resistance, as provided by the design codes, exhibited better structural performance than the analytic predictions that assumed perfect bonding. Further studies should examine the resistance of welded anchors in more depth.

For the purpose of the present study, one full-size and well-made hybrid girder for each considered case was sufficient to investigate the tendency in the behavioral characteristics of the hybrid girder. Further study with a larger number of specimens should be conducted based upon the results of this research and to allow statistical evaluation enabling to derive more reliably the best design solution for the steel-to-concrete connection of the hybrid girder.

Acknowledgements

This research was financially supported by the Korean Ministry of Environment as 'Public Technology Program Based on Environmental Policy' (2016000700003). This work was also supported by the Gachon University research fund of 2017 (GCU-2017-0205).

REFERENCES

[1] Sétra, Steel-Concrete Composite Bridges – Sustainable Design Guide, Sétra, 2010.
[2] M. Virlogeux, Recent evolution of cable-stayed bridges, Eng. Struct. 21 (1999) 737–755.
[3] Y. Yanaka, T. Tazakawa, N. Hirahara, Erection of the Tatara Bridge's superstructure, IABSE Symposium Reports vol. 79 (1998) 75–80.

[4] D. Yoo, J.S. Ko, C. Moon, Design of Cheong-Poong (steel-concrete hybrid cable-stayed) bridge, IABSE Symposium Reports vol. 96 (2009) 63–72.
[5] Y. Cheng, X. Nie, J. Fan, Structural performance and strength prediction of steel-to-concrete box girder deck transition zone of hybrid steel-concrete cable-stayed bridges, J. Bridge Eng. 21 (11) (2016), http://dx.doi.org/10.1061/(ASCE)BE.1943-5592.0000958.
[6] H.L. Wang, X.L. Ma, S.F. Qin, Study on the joint part of self-anchored cable-stayed suspension bridge with hybrid girder, Int. J. Adv. Comput. Technol. 5 (4) (2013) 158–163.
[7] F. Qin, J. Di, J. Dai, W. Lu, M. Zhao, Study on rational position of joint section of0020steel-concrete hybrid girder bridge, Adv. Mater Res. 671–674 (2013) 1007–1011.
[8] B. Park, Design of Joint in Hybrid Girder Combining Steel and PSC Members. Doctoral Dissertation, Department of Civil and Environmental Engineering, Seoul National University, 2016.
[9] S.E. Kim, H.T. Nguyen, Evaluation of the connection efficiency of hybrid steel-concrete girder using finite element approach, Int. J. Mech. Sci. 61 (2012) 8–23.
[10] J. He, Y. Liu, B. Pei, Experimental study on the steel-concrete connection in hybrid cable-stayed bridges, J. Perform. Constr. Facil. 28 (3) (2014) 559–570.
[11] J.Y. Oh, D.H. Lee, S.H. Cho, H. Kang, H.C. Cho, K.S. Kim, Flexural behavior of prestressed steel-concrete composite members with discontinuous webs, Adv. Mater. Sci. Eng. 278293 (2015) 13.
[12] P. Kozioł, M. Kożuch, W. Lorenc, S. Rowinski, Connection capacity of the transition zone in steel-concrete hybrid beam, Civil Environ. Eng. Rep. 25 (2) (2017) 137–146.
[13] Korea Concrete Institute (KCI), Structural Concrete Design Code, 2012.
[14] E. Hognestad, Ultimate strength of reinforced concrete in American design practice,London, UK, May, Proc. Symposium on the Strength of Concrete Structures 1956.
[15] C. Orangun, J. Jirsa, J. Breen, A reevaluation of test data on development length and splices, ACI Struct. J. 74 (3) (1977) 122–144.
[16] American Concrete Institute, ACI 408R-03. Bond and Development of Straight Reinforcing Bars in Tension, vol. 408, ACI Committee, 2003. p. 49.
[17] European Committee for Standardization, CEN 1994-4-4. Eurocode-4: Design of Composite Steel and Concrete Structures, Part 1-1: General Rules and Rules for Buildings, CEN, 2004.
[18] European Committee for Standardization, CEN 1994-2. Eurocode-4: Design of Composite Steel and Concrete Structures, Part 2: General Rules and Rules for Bridges, CEN, 2005.
[19] American Association of State Highway and Transportation Officials (AASHTO), AASHTO LRFD Bridge Design Specifications, 4th edition, 2007 Washington D.C..